Rising behaviour of single bubbles in narrow rectangular channels in Newtonian and non-Newtonian liquids

Abbreviated title:

Bubbles rising in a confined geometry

Lutz Böhm[a]*, Tokihiro Kurita[b], Katsuki Kimura[b], Matthias Kraume[a]

[a] *Chair of Chemical and Process Engineering, Technische Universität Berlin, Sekr. FH 6-1, Strasse des 17. Juni 135, 10623 Berlin, Germany, matthias.kraume@tu-berlin.de*

[b] *Graduate School of Engineering, Hokkaido University, N13W8, Sapporo 060-8628, Japan, tokihiro.kurita@gmail.com, kkatsu@eng.hokudai.ac.jp*

*corresponding author: phone: +49/30/31472791 fax: +49/30/31421134 email: lutz.boehm@tu-berlin.de

Abstract:

A phenomenological investigation of single bubbles ascending in a confined geometry with a rectangular cross section was done. Motivated by the goal to get a deeper understanding of the bubble behaviour in flat sheet membrane modules used in membrane bioreactors, the parameters channel depth (=spacing, 5-7 mm), bubble size (3-9 mm), superimposed liquid velocity (0-23.5 cm/s) and rheology of the continuous phase (Newtonian, shear-thinning) were varied. The shear-thinning liquid was used to simulate the rheological behaviour of activated sludge apparent in membrane bioreactors. The analysed properties included the rising paths, bubble shape, absolute and relative terminal rise velocities, friction factors and oscillation frequencies and amplitudes of the bubble.

As expected, a significant influence of the rheology of the continuous phase was found on the rising behaviour. In the shear-thinning liquid, the bubbles followed mostly a straight rising path with negligible oscillations. The variation of the channel depth mainly had an influence on the terminal rise velocity of

the bubbles ascending in the shear-thinning liquid with higher values in the channel with the larger channel depth. Increasing the bubble size led to higher rising velocities and to enhanced oscillations.

Keywords:

single bubbles; non-Newtonian liquid; confined geometry; terminal rise velocity; oscillation frequency

1 Introduction

The phenomenological investigation of the fluid dynamic behaviour of fluid particles ascending or descending in a continuous phase is of particular interest for a broad range of fields in engineering. In chemical engineering, droplets and bubbles appear in numerous unit operations such as mixing of disperse systems or bubble columns. This work is motivated by the aeration of flat sheet membrane bioreactors. The aeration is applied, inter alia, to clean the membrane surfaces [1]. Usually, flat sheet membrane bioreactors are operated as cross-flows where the (aerated) suspension flows along the membrane surface. During filtration, a deposition layer is growing on the filtration surfaces. The inserted bubbles induce flows in the liquid phase that generate shear stresses on the membranes that help cleaning off these deposition layers. Such systems contain a certain number of membranes which are stacked in modules. The flat sheet membranes have a defined spacing between each other that is called channel depth in the following. These membrane systems are often arranged as air lift loop reactors with a bubble swarm rising between the membrane plates and a non-aerated downcomer area for the recirculating liquid phase. This system, with a certain number of channels between the membranes and a bubble swarm rising between them, is fairly complex. As no phenomenological investigation for a single bubble rising in a channel with a rectangular cross section in the dimensions found in flat sheet membrane bioreactor systems can be discovered in literature, this work builds the foundation for future bubble swarm experiments.

While Clift et al. [2] and Chhabra [3] gave a broad overview of the motion of particles in Newtonian and non-Newtonian liquids, Table 1 assembles publications from authors dealing with single bubble movement in more or less confined geometries, mostly with rectangular cross sections, investigated with high speed cameras. This measurement technique is usually called shadowgraphy. These are sorted alphabetically and by the working groups. Here, rectangular cross sections can be found with channel depth down to 1 mm [4]. The camera resolutions were up to $4*10^6$ pixel [5], with frame rates ranging from 6 Hz [6] up to 1 kHz [7, 8]. Fujiwara et al., Sanada et al. and Zaruba et al. [8-10] used two cameras arranged perpendicular to each other, e.g., for a 3D reconstruction of the bubble shape or rising path. The varied parameters were in most cases geometrical properties, the bubble size (ranging from 0.3 mm [11] up to 45 mm [12] or even Taylor bubbles [13]) and viscosity of the continuous phase, including the usage of non-Newtonian liquids. The measured quantities were usually the terminal rise velocity, the bubble shape and the rising path.

Figueroa-Espinoza et al. [26] discussed the effect of confinement on the bubble motion for Reynolds numbers below 500 and bubble diameter to gap width ratios s smaller than 0.38 (in this investigation, s is larger than 0.43 for all and above 1 in most cases). They found a strong dependence of the friction factor on this ratio with a friction factor enhancement proportional to a factor times s to the power of three in the investigated range. In their case, the factor depended on the Reynolds number differing by an order of magnitude with the lower factor for rectilinear rising bubbles with Reynolds numbers below 70 and vice-versa for oscillating bubbles with Reynolds numbers above 70 (it is worth mentioning that this Reynolds number is below the values usually mentioned for beginning oscillatory movement which is often related to the Morton number).

In earlier publications by the authors, the focus was on the wall shear stress induced by the single bubble flow measured with the electrodiffusion method as this is usually regarded as the crucial property for the cleaning process [14]. Additionally, the liquid flow around the bubble was measured with particle image velocimetry [15]. This article shows the results of a parameter study motivated by the membrane application and performed with a high speed camera. Here, a comparison of the results for a varied channel depth, bubble size, superimposed liquid velocity and liquid phase viscosity was done and its results were put into context with mathematical models known from literature. It is worth mentioning that most of these mathematical models were developed for free rising bubbles. Therefore, here it was possible to determine the influence of the confined geometry. Additionally, it is worth mentioning that another goal of this work was to compare investigations done with water – as it was often done for fluid dynamic investigations of membrane systems – with experiments performed under the same conditions but in a system that had similar rheological characteristics as the real activated sludge system.

2 Materials and Methods

For the optical measurements done in this study, two different rectangular acrylic glass channels (Fig.1a) with a width of 160 mm and a height of 1500 mm were constructed which only differed in their channel depths (z-dimension). A detailed description of the fully automated apparatus (Fig.1b) can be found in Böhm et al. [14]. During one measurement run, air was inserted into the channel at the bottom with the help of a syringe pump Harvard Apparatus Pump 11 Elite™ together with a Hamilton Gastight® syringe and a defined gas volume was collected in a cup. The cup was fixed on a rotatable rod and the bubble was released by turning the cup with the help of a servo motor located outside of the channel. With the help of a centrifugal pump a co-current, superimposed liquid velocity could be adjusted. The bubble rose and left

the channel at the top through a bubble separator. Completely controlled with NI LabVIEW, for statistical reasons this was done 50 times for one channel depth (5 or 7 mm), one bubble size (3 to 9 mm) and one superimposed liquid velocity (0 to 23.5 cm/s) in deionized water or a shear thinning liquid. As shear thinning liquid, a transparent XanthanTER2000 solution (in the following called Xanthan solution) with a concentration of 0.8 g/L was used. Its rheological behaviour can be described by an Ostwald-de Waele approach with a flow consistency index of K=0.166 $Pas^{0.48}$ and a flow behaviour index of n=0.48 (measured with an Anton Paar RheolabQC in a shear rate range from 5 to 950 1/s). Depending on the shear rate, the viscosity of the Xanthan solution was one to two orders of magnitudes higher than in water. No viscoelasticity was measured for the Xanthan solution (which with the given measurement system meant no or very low viscoelasticity). This simulates a typical activated sludge in a membrane bioreactor [16]. The investigated parameter combinations and the according symbols used in the diagrams can be found in Table 2. Additionally, the table shows the symbols for simulations performed with computational fluid dynamics (CFD) which were compared to the experiments. These were in parts already discussed in Prieske et al. [17]. In Prieske et al.'s CFD calculations [17], the Volume-of-Fluid-method for the multiphase calculations done with Ansys Fluent© was used. A user defined function was developed to move a fine meshed area near the bubble with the bubble during its ascent in the domain. The used geometry was comparable to the channel shown in Fig.1a with the exception that due to symmetry reasons, only half of the channel depth and therefore also only half of the bubble was calculated.

In the experiments, the ascent of the bubble was recorded with an 8bit Photonfocus MV-D752 high speed camera at a frame rate of 200 Hz with a resolution of 148 by 582 pixel in the x-y-plane (e.g., Fig.2a or b) or 100 by 582 pixel in the y-z-plane (e.g., Fig.2c or d), respectively. For the image analysis, NI Vision Development Module and ImageJ were used and further statistical analysis was done with MS Excel. In most cases, the standard deviations of the determined values were so small that these are left out in the following diagrams.

3 Results and Discussions

3.1 Rising paths

Figures 2a-d show each an exemplary rising path of a bubble in the front (x-y-plane) and side view (y-z-plane) by overlaying a series of recorded images. Figure 2a shows the rising path of a bubble with an

equivalent diameter larger than the channel depth in water in the front view. Deformations are strongly pronounced. The deformation and the according flow field in the liquid near the bubble (with a Kármán vortex street in the wake, further described in [15]) led to an oscillation as commonly known for bubbles of the given size rising in water in an unconfined geometry (following Clift et al.'s shape regime map [2] all bubbles investigated in water were in the 'wobbling' bubble shape region). Here, due to the confining walls, only a 2D-zig-zag-movement was apparent. Figure 2b shows for the same conditions the ascent of a bubble in the Xanthan solution. Apparently, a constant shape of the bubble is visible which goes along with a straight rising path (all bubbles investigated in Xanthan solution were in the 'ellipsoidal' bubble shape region in the mentioned shape regime map).. The according symmetrical flow field of the liquid near the bubble can be found in Böhm and Kraume [15], as well.

Figure 2c shows the rising path of a bubble with an equivalent diameter smaller than the channel depth in water in the side view. Although the movement was hindered by the walls as well, an oscillating movement was visible. As the recordings in the front view showed an oscillation as well (not shown here), the bubble takes a helical path in this case. Figure 2d shows the rising path of a bubble for the same parameter combination in Xanthan solution. As it was found in the front view for the larger bubble, for the small bubble in the side view as well, a straight rising path was apparent. This characteristic reflects the effect of the viscosity on the flow field near the bubble.

3.2 Rising velocity

Figure 3a shows the absolute terminal rise velocities w_{abs} in water over the bubble size together with the well-known rise velocities for bubbles rising in pure and contaminated water in unconfined geometries [2]. The standard deviation of each data point is too small to be visible in the diagram. A clear distinction between three velocity levels is possible. These velocity levels are due to the superimposed liquid velocities. For the parameter combinations tested in water, three cases are discussed in the following section where each time one parameter is varied and two parameters are kept constant. For all parameter combinations, increasing the bubble size (in the range investigated here) did not lead to significant changes in the rising velocity. This behavior can be expected as the data from Clift et al. [2] indicated. Still, in pure unconfined systems due to the beginning of bubble deformation in the range from 1.4 mm up to approximately 6 mm bubble diameter, a decrease of the rising velocity was found. In this project's investigated system, a wall effect was apparent. Still, the tendency is visible that the rising velocity first decreases with the bubble diameter and then from a 5 mm bubble diameter on increases again.

Comparing the results for the same bubble size and superimposed liquid velocity, the results for the two different tested channel depths differ in maximum by 5%. Especially for the cases without superimposed liquid velocity, the bubbles ascent faster in the channel with a channel depth of 7 mm which can be due to the lower grade of confinement. With superimposed liquid velocity, the trend is not as clear.

Varying only the superimposed liquid velocity, an increase of the liquid velocity led to higher bubble rise velocities. In general, one would expect approximately a terminal rise velocity that adds up from the terminal bubble rise velocity without superimposed liquid velocity and the applied superimposed liquid velocity in each case. This calculation can be used as a first estimate. However, in these cases where the bubble diameter was smaller than the channel depth, the terminal bubble rise velocity was higher than the expected value from the mentioned estimation. This is most likely due to the fact that the given value of the superimposed liquid velocity is equal to the superficial liquid velocity in the channel. In reality, not a constant liquid velocity value is apparent over the channel depth but a liquid velocity profile. Therefore, the smaller bubbles, that had the tendency to rise in the center of the channel, rose in a range of higher velocities (here: maximum velocity in water approx. 1.5 times superficial liquid velocity; in Xanthan solution approx. 1.3 times superficial liquid velocity [15, 18]).

Regarding the CFD results, the numerical values of the rise velocities differed by 9.4% in average. The difference was mainly due to the fact that in the simulations only half of the channel depth was taken into account and a symmetry plane was placed in middle between the two walls in the x-y-plane (further description in Prieske et al. [17]). This was especially crucial for the cases with bubble diameters smaller than the channel depth as in these cases the oscillation of the bubble in the y-z- plane was suppressed.

For bubbles rising in non-Newtonian liquids, Chhabra [3] gave a broad overview. The behavior of the terminal rise velocity is not as clear in this case as it is in water. With increasing bubble size, the terminal rise velocity increases as well, up to a certain bubble size from which on either the slope of the increase is reduced or the bubble rise velocity is even constant. In some cases, this change of the rise behavior is not a continuous function but goes along with a step of the velocity to a higher value at a certain bubble size. Margaritis et al. [19] presented data for bubbles rising in Xanthan solutions of different concentrations. From a bubble diameter of approximately 4 mm on, for all Xanthan concentrations a constant terminal rise velocity of approximately 0.27 m/s was found. In general, in the investigated case even with a viscosity up to two orders of magnitudes higher than that of water, the rise velocities are still in the same range as in water differing mainly for small bubbles and the parameter combinations without superimposed liquid velocity. In Fig. 3b, for the investigated cases without liquid velocity, the rise

velocities first increase and from a bubble size of 5 mm on, the values are constant or even decrease slightly. In comparison to the data from Margaritis et al. [19], the constant values are lower by approximately 30% for the 7 mm channel and 45% for the 5 mm channel. The confining walls had two counteracting effects that resulted from the higher appearing velocity gradients (=shear rates). On the one hand side, the walls led to higher friction in the system and on the other hand, the higher shear rates led to a lower viscosity due to the shear-thinning effect. As the rise velocities were lower in comparison to the free rising bubble, the higher resistance obviously exceeded the beneficial effect of the lower viscosity which was still higher than the one of water. For the parameter combinations with superimposed liquid velocity, there were again three different velocity levels (actually there are five levels but 10 and 12.5 cm/s and 20 and 23.5 cm/s are too close to be clearly differentiated). Here, even from a bubble size of 5 mm on, the rise velocity was not constant but steadily increasing.

Generally the values are in good agreement with experiments done at the authors' laboratory in a comparable apparatus [20]. In these tests, no superimposed liquid velocity was applied but, in addition to the tests in water, they used real activated sludge from a membrane bioreactor in contrast to the Xanthan solution used in this investigation.

As in many correlations the relative bubble rise velocity $w_{B,rel}$

$$w_{B,rel} = w_{B,abs} - v_L \qquad \{[(1)]\}$$

(calculated from the subtraction of the superficial liquid velocity v_L from the absolute bubble rise velocity $w_{B,abs}$) is used e.g. for the bubble Reynolds number, these values were plotted in Fig. 4a for water and in Fig. 4b for the Xanthan solution. In all cases the relative rise velocities for the parameter combinations with superimposed liquid velocity were consistently higher than the values without superimposed liquid velocity. There are several possibilities to explain this. Besides the changing deformation of the bubble, change of the flow behavior, differing viscosity conditions for the experiments in the shear thinning solution, the most important factor – as discussed earlier – is that the bubble was not rising in a liquid with a constant velocity value over the channel depth equal to the superimposed liquid velocity but in a liquid that had a certain velocity profile.

In a dimensionless form, Legendre et al. [21] correlated the bubble Reynolds number Re_B (where n=1 and $K=\mu_f$ for Newtonian liquids, d_B is the equivalent bubble diameter and ρ_f is the liquid density)

$$Re_B = \frac{w_{B,rel}^{2-n} d_B^n \rho_f}{K} \qquad \{[(2)]\}$$

(in this investigation, the Reynolds number ranged from 536 to 2175 for water and from 10 to 76 for the Xanthan solution; for completeness it is worth mentioning that the Eötvös number $Eo=g\Delta\rho d_b^2/\sigma$ with g as the gravitational acceleration and σ as the surface tension was between 1.2 and 13 for both liquids as the surface tension is σ=72.4mN/m and equal in both cases) with the Morton number Mo [3]

$$Mo = \frac{g^{3n-2}K^4}{\rho_f^{2-n}\sigma^{n+2}} \qquad \{[(3)]\}$$

(the Morton numbers for the given investigation are $Mo=2.55*10^{-11}$ for water and $Mo=3.9*10^{-6}$ for the Xanthan solution) and the Weber number

$$We = \frac{\rho_f w_{B,rel}^2 d_B}{\sigma} \qquad \{[(4)]\}$$

(with Weber numbers between 1.3 and 7.2 for both liquids) where the two latter ones are correlations related to the deformation of the bubble. Legendre et al. [21] showed a good fit of experimental data for the correlation

$$Re_B = 2.05We^{2/3}Mo^{-1/5} \qquad \{[(5)]\}$$

In Fig.5, this investigation's data is presented together with eq. (5). Roughly, the linear slope relating the bubble Reynolds number with the factor $We^{2/3}Mo^{-1/5}$ can be found for both value ranges here as well, where the lower range shows the data for bubbles rising in Xanthan solution and the upper range shows the data for bubbles rising in water. While the correlation slightly overestimated the experimental values for the bubble rising in non-Newtonian liquid, it underestimated the experimental values for the ascent in water. In spite of the wall effect and rheological difference for the Xanthan solution in comparison to water in the given system, qualitatively the correlation is overall still in good agreement with the experimental data found in this investigation. Quantitatively, an average difference between the theoretical and experimental value of 46% for water and 22% for the Xanthan solution was found. A regression to adjust the prefactor (Legendre et al.: 2.05) and the exponent of the Weber number (Legendre et al.: 2/3) provided for water $Re_{B,N,adj}=3.295We^{0.806}Mo^{-1/5}$ with a coefficient of determination of 0.97 and for the Xanthan solution as continuous phase $Re_{B,nN,adj}=1.846We^{0.601}Mo^{-1/5}$ with a coefficient of determination of 0.99. The increase of the prefactor and exponent in the case of water can be ascribed to the wall effect (although it is worth mentioning that in Legendre et al. [21], the correlation is only applied to $We^{2/3}Mo^{-1/5}$ up to 300 and approximately half of the values for water in the given case were above this

value) while the decrease of the prefactor and exponent in the case of the Xanthan solution can be ascribed to wall and rheological effects.

3.3 Friction factor and eccentricity

The friction factor for bubbles rising in water in unconfined geometries is widely discussed in literature (e.g. [2]). For the mentioned motivation of this project, aerated membrane bioreactors, the friction factor of the bubbles (as well as the corresponding bubble rise velocity) is of interest as it correlates to the cleaning potential of the bubble and to the retention time of the bubble in the system.

The friction factor C_D is usually calculated as

$$C_D = \frac{4}{3}\frac{|\rho_B - \rho_f|}{\rho_f}\frac{g d_B}{w_{B,rel}^2} \qquad \{[(6)]\}$$

(with ρ_B as the density of the bubble) and plotted over the bubble Reynolds number Re_B. The describing curve of the friction factor over the bubble Reynolds number can be separated into three zones with a decreasing part for spherical bubbles, a transition zone often related to a Morton number with starting bubble deformation accompanied by an increasing part ending up in a constant value (Fig.6a). Different correlations can be found in literature for bubbles rising in Newtonian liquids but roughly all of these are comparable to the following four equations [22, 48] (where eq. (7b) is a variation of the well-known Hadamard-Rybszynski-equation eq. (7a) for fluid particles in Newtonian liquids)

$$C_{D,N} = \frac{24}{Re_B} Y \quad \text{with} \quad Y = \frac{2}{3} \text{ for bubbles in Newtonian liquids} \qquad \{[(7a)]\}$$

$$C_{D,N} = \frac{16}{Re_B} + \frac{14}{Re_B^{0.78}}\left(\frac{1}{1 + 10 Re_B^{-0.6}}\right) \text{ for } Re_B < \left(\frac{768}{Mo}\right)^{\frac{1}{5}} \text{ (spherical bubbles)} \qquad \{[(7b)]\}$$

$$C_{D,N} = \frac{Mo Re_B^4}{48} \text{ for } \left(\frac{768}{Mo}\right)^{\frac{1}{5}} < Re_B < \left(\frac{125.28}{Mo}\right)^{\frac{1}{4}} \qquad \{[(8)]\}$$

$$C_{D,N} = 2.61 \text{ for } Re_B > \left(\frac{125.28}{Mo}\right)^{\frac{1}{4}}. \qquad \{[(9)]\}$$

All experimental results calculated with eq. (2) and (6) are shown in Fig.6a. The friction factor values for water are in the transition region for deformed bubbles scattered around the transition curve defined by eq. (8) ending up in an upper bound that agrees with the constant friction factor value for the ascent in unconfined geometries. Generally, the values for the parameter combinations with superimposed liquid

velocity are lower than the ones found for the cases without liquid velocity. This is a result of the higher relative terminal rise velocities. The results for Xanthan solution as continuous phase are in a lower value range of Reynolds numbers. The friction factor values itself are approximately in the same range as the experimental values found for water. However, in comparison to the correlation for Newtonian liquids, the friction factors are higher which correlates to the lower relative terminal rise velocities at much higher viscosities. A regression for all experimental results in Xanthan solution with 3 mm bubbles (which correlate to the lowest Reynolds number found for each combination of channel depth and superimposed liquid velocity) gives a correction factor in eq. (7a) of Y=1.61. This correction factor is rather high in comparison to values in literature for bubbles rising in shear-thinning liquids with a flow behaviour index of n=0.48 (the Y value is usually below 1 for low Reynolds numbers and in the case of higher Reynolds numbers in the range of 1.2) [3]. Although not done for bubbles rising in non-Newtonian liquids, defining a transition range as defined by eq. (8) for the non-Newtonian liquid as well, the deformation obviously starts already at lower bubble Reynolds numbers.

As the described behaviour for bubbles rising in non-Newtonian liquids is not generally the same for all types of liquids, here one correlation is shown as an example for results of investigations with carboxymethyl cellulose (CMC) and Xanthan solution as continuous phase. Margaritis et al. [19] used in their correlation a modified bubble Reynolds number $Re_{B,h}$

$$Re_{B,h} = \frac{w_{B,rel}^{2-n} d_{B,h}^{n} \rho_f}{K} \qquad \{[(10)]\}$$

that is not calculated with the equivalent but with the horizontal dimension of the bubble $d_{B,h}$. Based on experimental data, the modified friction factor $C_{D,h}$ has to be calculated as

$$C_{D,h} = \frac{4}{3} \frac{|\rho_B - \rho_f|}{\rho_f} \frac{g d_B^3}{w_{B,rel}^2 d_{B,h}^2} \qquad \{[(11)]\}$$

where the resistance is related to a circular projected area of the bubble with a diameter equal to the horizontal diameter. The describing correlations for the friction factor $C_{D,nN}$ are then calculated as

$$C_{D,nN} = \frac{16}{Re_{b,h}} \left(1 + 0.173 Re_{B,h}^{0.657}\right) + \frac{0.413}{1 + 16300 Re_{B,h}^{-1.09}} \quad \text{for } Re_{b,h} < 60 \qquad \{[(12)]\}$$

$$C_{D,nN} = 0.95 \text{ for } Re_{B,h} > 60 \qquad \{[(13)]\}$$

Based on this thought, the horizontal ($d_{B,h}$) and vertical dimensions of the bubbles ($d_{B,v}$) were analysed. The analysis was done for the images of the x-y-plane. The values are compared to results presented by

Miyahara and Yamanaka [23] for bubbles rising in an unconfined geometry. In many publications, the eccentricities were discussed using the terms major and minor axis. Unfortunately it is not always clear what was used in the equations as major and the minor axis. In Miyahara and Yamanaka [23], the horizontal dimension of the bubble was always called major axis independent of the fact if it was larger or smaller than the vertical dimension which was always called minor axis. This nomenclature is kept in the following. The main differences to the investigations from Miyahara and Yamanaka [23] are that in their investigation, the geometry did not influence the bubble and that no superimposed liquid velocity was apparent. Therefore, in this investigation, the terms horizontal and vertical dimensions are used in contrast to horizontal and vertical diameters as, due to the walls, e.g., the horizontal diameter is not constant in the x-z-plane (=bubble cross section not circular). Nevertheless, in the following the horizontal dimension of the bubble in the x-y-plane is used for the calculations. Both mentioned factors influenced the bubble shape while, especially for the non-Newtonian liquid phase, the main difference was visible between the cases with and without liquid velocity independent of the actual value of the liquid velocities for bubbles larger than 3 mm. Figure 7a shows the values of the minor axis divided by the major axis over the bubble Reynolds number Re_B for water. The values are in a range between 0.6 and 1, decreasing with increasing bubble Reynolds number. Miyahara and Yamanaka [23] also reported only of ratios below 1 for bubbles in water. It is worth mentioning that the determination of the eccentricity of a deformable bubble (see also Fig. 2a) is challenging. The values shown here are averaged values of constantly changing horizontal and vertical dimensions in several oscillation periods. As it is not clear, how exactly Miyahara and Yamanaka [23] determined the horizontal ($d_{B,h}$) and vertical dimension ($d_{B,v}$) of the bubble, it cannot be stated with certainty if different results in both investigations are a result of the confining geometry or differing ways of analysing the images. Still, in some cases, it is clear that the walls influence the bubble shape by forcing the bubble independent of its size to rise in a – if not straight – rocking zig-zag motion in the x-y-plane which was accompanied by a differing bubble shape in comparison to that of a free rising bubble which in some case would rise on a helical path. In Fig.7b, the results of the minor axis divided by the major axis of the (here mostly non-oscillating) bubble found in Xanthan solution is plotted and related to a correlation [23]. In contrast to the correlation, here the values of the ratio were constant up to approximately $Re_B Mo^{0.078}=15$ at a ratio value of 1. As for the correlation, the ratio decreases for higher values of $Re_B Mo^{0.078}$.

Using the determined horizontal dimensions, Fig.6b was assembled with the help of eq. (10) and (11). The experimental values scatter around the correlation described in eq. (12) and (13). Especially for the

results in Xanthan solution, the experimental results follow the trend described in eq. (12) fairly well. The results found in water show a larger variation around the terminal value described by eq. (13). It is worth mentioning that in Margaritis et al. [19] especially in the transition region (roughly in the range $20<Re_{b,h}<1000$), which in the correlation is given as a transition point at Re=60, the scattering of the experimental values around the correlation is in the same range as found in the authors' experiments. Adjusting eq. (12) by a factor of 1.07,

$$C_{D,nN,adj} = 1.07\left(\frac{16}{Re_{b,h}}\left(1+0.173Re_{B,h}^{0.657}\right)+\frac{0.413}{1+16300Re_{B,h}^{-1.09}}\right) \qquad \{[(14)]\}$$

for the investigated range of Reynolds numbers in Xanthan solution of up to approximately Re=100, a new describing correlation for the adjusted friction factor $C_{D,nN,adj}$ was found with a coefficient of determination R^2=0.8. Although only a rough assumption, it can be assumed that for higher Reynolds numbers (in water), the values would also converge to the value of 0.95 for the friction factor described by eq. (13).

3.4 Oscillation frequency and amplitude

Due to the deformation and the rocking nature of the bubble ascent in the investigated bubble size range, the parameters frequency and amplitude of the oscillation (here in the x-y-plane) were worth investigating as well. In Fig.8, the oscillation amplitude A is plotted over the oscillation frequency f_B. All oscillation frequencies were higher than 5 Hz. All frequencies above 15 Hz had very low amplitudes which in combination made the oscillations for these combinations negligible. For water, the parameter combinations without superimposed liquid velocity in a channel with 5 mm depth showed the widest variety with the highest amplitude and lowest frequency for the largest bubble and the lowest amplitude and highest frequency for the smallest bubble. The parameter bubble size is not directly visible in the diagram. However, in general, for water it can be stated that with increasing bubble size the oscillation frequency was reduced and the oscillation amplitude was raised. The influence of the superimposed liquid velocity established in a reduction of the amplitude while the frequency stayed almost the same. For many parameter combinations with the larger channel depth, the amplitudes were higher than for the according parameter combination in the smaller channel while the frequency was equal or slightly smaller.

As it was already indicated in section 3.1 discussing the rising paths, for bubbles rising in Xanthan solution in most cases no oscillation was visible to the unaided eye. The image analysis basically confirmed quantitatively as well this qualitative prediction as, e.g., in all cases without superimposed

liquid velocity the amplitude of the oscillation was below 0.2 mm. In most cases with superimposed liquid velocity, independent of the actual value, the amplitude was in the range of 0.8 to 1.0 mm. The variation of all other parameter had a negligible influence or did not show a clear relation.

The oscillation frequency is often presented using the dimensionless Strouhal number St

$$St = \frac{f_B d_B}{w_{B,rel}} \qquad \{[(15)]\}$$

calculated with the bubble oscillation frequency f_B. Miyahara and Yamanaka [23] calculated the Strouhal number St_h with the horizontal dimension of the bubble

$$St_h = \frac{f_B d_{B,h}}{w_{B,rel}} \qquad \{[(16)]\}$$

and introduced a correlation for this Strouhal number for free rising bubbles in Newtonian and non-Newtonian liquids St_{Miya}

$$St_{Miya} = 0.0229\left(Re_{B,h}Mo^{0.26}\right)^{2.18-0.38211\ln\left(Re_{B,h}Mo^{0.26}\right)} \qquad \{[(17)]\}$$

with $Re_{B,h}$ as described in eq. (10). Figure 9 shows the correlation together with the experimental values found in this investigation. It is worth mentioning that this equation was determined for values of $Re_{B,h}Mo^{0.26}$ above 2 and that their experimental values scattered significantly around the curve described by eq. (17). This investigation's values of $Re_{B,h}Mo^{0.26}$ were in half of the cases below 2. The experimental results for water followed a comparable trend but still all Strouhal numbers were higher than the ones found by Miyahara and Yamanaka. The adjusted Strouhal correlation $St_{adj,N}$

$$St_{adj,N} = 0.66\left(St_{Miya}\right)^{0.51} \qquad \{[(18)]\}$$

describes the trend for bubbles rising in water with a coefficient of determination of R^2=0.94. The Strouhal numbers for the bubbles rising in Xanthan solution were also higher in comparison to Miyahara and Yamanaka's results but generally the values also followed the trend to increase with increasing values of $Re_{B,h}Mo^{0.26}$. As mentioned above, in parts, the frequencies were fairly high and the amplitudes fairly low so that generally the trend was not as clear as for bubbles rising in water. Therefore, the values found in Xanthan solution were not included in the regression to determine eq. (18).

Relating the information from Fig.8 and 9, Figure 10 shows a relation of the dimensionless amplitude A*

$$A^* = \frac{A}{d_B} \qquad \{[(19)]\}$$

(calculated with the amplitude A) to the Strouhal number as calculated by eq. (15). The general trend showed an exponential decline with increasing Strouhal number. An exponential fit provided the correlation describing the dimensionless amplitude

$$A^* = 0.0145 St^{-1.52} . \qquad \{[(20)]\}$$

Still, it is worth mentioning that the experimental data scattered around the correlation leading to a fairly low coefficient of determination of R^2=0.55. Therefore, the idea of relating the dimensionless amplitude with the Strouhal number should be further investigated in the future to achieve a more accurate correlation.

4 Summary and Conclusions

The purpose of this work was the phenomenological investigation of single bubbles ascending in a confined geometry with a rectangular cross section. Motivated by the goal to get a deeper understanding of the bubble behaviour in flat sheet membrane modules used in membrane bioreactors, the parameters channel depth, bubble size, superimposed liquid velocity and rheology of the continuous phase were varied. Besides water, a non-Newtonian Xanthan solution was used as continuous phase to simulate the rheological behaviour of activated sludge apparent in membrane bioreactors. The analysed parameters included the rising paths, the absolute and relative terminal rise velocity, the friction factor, the eccentricity of the bubble and the frequency and amplitude of the oscillating bubble. Where applicable, these properties were also included in dimensionless numbers, put in context with literature and new correlations were determined.

As expected, a significant influence of the rheology of the continuous phase was found. In contrast to the rising behaviour of the bubbles in water, in Xanthan solution the bubbles followed mostly a straight rising path with negligible oscillations which was accompanied by a stable bubble shape and a slightly lower rising velocity. The variation of the channel depth mainly had an influence on the terminal rise velocity of the bubbles ascending in the Xanthan solution. Higher values were found for most bubbles rising in the channel with the larger channel depth. As expected, increasing the bubble size led to higher rise velocities and, especially in water, it led to enhanced oscillations. In comparison to the ascent in stagnant water, with superimposed liquid velocity the bubbles had higher relative terminal rise velocities independent of the actual value of the liquid velocity. With additional liquid velocity, the oscillation of the bubble was generally damped in water. In the shear-thinning Xanthan solution on the other hand, the superimposed

liquid velocity led to higher shear rates appearing in the confined flow region ending up in lower liquid viscosities. This effect eventually led to stronger - but in comparison to water still minor - oscillation of the rising path during the ascent and therefore a change in the rising behaviour.

Finally, it can be concluded, that while the channel depth does not generally have a significant influence, the rheology of the continuous phase is a parameter that should not be disregarded in fluid dynamical research of membrane bioreactors.

Acknowledgments

This work is part of the Collaborative Research Centre "Integrated Chemical Processes in Liquid Multiphase Systems" coordinated by the Technische Universität Berlin. Financial support by the Deutsche Forschungsgemeinschaft (DFG, SFB/TR 63 and KR 1639/18-1) and the Deutsche Akademische Austauschdienst (DAAD, D/10/46059) is gratefully acknowledged. Special thanks for the support during the work go to Manuel Brehmer, Andrea Hasselmann, Sascha Pietsch, Helmut Prieske, Paul Schallau and Kenny Sowerwine.

References

[1] L. Böhm, A. Drews, H. Prieske, P. Bérubé, M. Kraume, The importance of fluid dynamics for MBR fouling mitigation, Bioresour. Technol. 122, (2012) 50-61. doi: 10.1016/j.biortech.2012.05.069.

[2] R. Clift, J. Grace, M. Weber, Bubbles, Drops and Particles, Academic Press New York, 1978.

[3] R. Chhabra, Bubbles, drops, and particles in non-Newtonian fluids, CRC Boca Raton, 2006.

[4] M. Roudet, V. Roig, A.-M. Billet, F. Risso, Paths and shapes of two-dimensional rising bubbles at high-Reynolds number, Proceedings of the ICMF 2007, 6th International Conference on Multiphase Flow, 2007.

[5] M. J. Sathe, J. B. Joshi, G. Evans, Characterization of Turbulence in Rectangular Bubble Column, Chem. Eng. Sci. 100, (2013) 52-68. doi: 10.1016/j.ces.2013.01.004.

[6] D. Dekée, P. Carreau, J. Mordarski, Bubble velocity and coalescence in viscoelastic liquids, Chem. Eng. Sci. 41, 9 (1986) 2273-2283. doi: 10.1016/0009-2509(86)85078-3.

[7] K. Ellingsen, F. Risso, On the rise of an ellipsoidal bubble in water: oscillatory paths and liquid-induced velocity, J. Fluid Mech. 440, (2001) 235-268. doi: 10.1017/S0022112001004761.

[8] T. Sanada, M. Shirota, M. Watanabe, Bubble wake visualization by using photochromic dye, Chem. Eng. Sci. 62, 24 (2007) 7264-7273. doi: 10.1016/j.ces.2007.08.037.

[9] A. Fujiwara, Y. Danmoto, K. Hishida, M. Maeda, Bubble deformation and flow structure measured by double shadow images and PIV/LIF, Exp. Fluids 36, 1 (2004) 157-165. doi: 10.1007/s00348-003-0691-0.

[10] A. Zaruba, D. Lucas, H.-M. Prasser, T. Höhne, Bubble-wall interactions in a vertical gas-liquid flow: Bouncing, sliding and bubble deformations, Chem. Eng. Sci. 62, 6 (2007) 1591-1605. doi: 10.1016/j.ces.2006.11.044.

[11] M. J. Sathe, I. H. Thaker, T. E. Strand, J. B. Joshi, Advanced PIV/LIF and shadowgraphy system to visualize flow structure in two-phase bubbly flows, Chem. Eng. Sci. 65, 8 (2010) 2431-2442. doi: 10.1016/j.ces.2009.11.014.

[12] B. G. M. van Wachem, J. C. Schouten, Experimental validation of 3-D lagrangian VOF model: Bubble shape and rise velocity, AIChE J. 48, 12 (2002) 2744–2753. doi: 10.1002/aic.690481205.

[13] C. Clanet, P. Héraud, G. Searby, On the motion of bubbles in vertical tubes of arbitrary cross-sections: some complements to the Dumitrescu–Taylor problem, J. Fluid Mech. 519, (2004) 359-376. doi: 10.1017/S0022112004001296.

[14] L. Böhm, A. Drews, M. Kraume, Bubble induced shear stress in flat sheet membrane systems - Serial examination of single bubble experiments with the electrodiffusion method, J. Membr. Sci. 437, (2013) 131-140. doi: 10.1016/j.memsci.2013.02.036.

[15] L. Böhm, M. Kraume, Comparison of the rising behavior of single bubbles in narrow rectangular channels in Newtonian and non-Newtonian liquids by serial examinations with Particle Image Velocimetry, J. Non-Newtonian Fluid Mech. submitted, (2014).

[16] S. Rosenberger, K. Kubin, M. Kraume, Rheology of Activated Sludge in Membrane Bioreactors, Eng. Life Sci. 2, 9 (2002) 269–275. doi: 10.1002/1618-2863(20020910)2:9<269::AID-ELSC269>3.0.CO;2-V.

[17] H. Prieske, L. Böhm, A. Drews, M. Kraume, Optimised hydrodynamics for membrane bioreactors with immersed flat sheet membrane modules (presented at the 5th IWA specialised membrane technology conference for water & wastewater treatment. Beijing, China), Desalin. Water Treat. 8, 1-3 (2010) 270-276. doi: 10.5004/dwt.2010.1784.

[18] J. Hartnett, M. Kostic, Heat transfer to Newtonian, non-Newtonian fluids in rectangular ducts, J. Hartnett, T. Irvine (Eds.), in: Advances in Heat Transfer, Elsevier, 1989, pp. 247-356.

[19] A. Margaritis, D. W. Bokkelte, D. G. Karamanev, Bubble rise velocities and drag coefficients in non-Newtonian polysaccharide solutions, Biotechnol. Bioeng. 64, 3 (1999) 257-266. doi: 10.1002/(SICI)1097-0290(19990805)64:3<257::AID-BIT1>3.0.CO;2-F.

[20] A. Drews, H. Prieske, E.-L. Meyer, G. Senger, M. Kraume, Advantageous and detrimental effects of air sparging in membrane filtration: Bubble movement, exerted shear and particle classification, Desalination 250, 3 (2010) 1083-1086. doi: 10.1016/j.desal.2009.09.113.

[21] D. Legendre, R. Zenit, J. Velez-Cordero, On the deformation of gas bubbles in liquids, Phys. Fluids 24, 4 (2012) 043303. doi: 10.1063/1.4705527.

[22] J. Harper, The motion of bubbles and drops through liquids, Adv. Appl. Mech. 12, 59 (1972) 129. .

[23] T. Miyahara, S. Yamanaka, Mechanics of Motion and Deformation of a Single Bubble Rising through Quiescent Highly Viscous Newtonian and Non-Newtonian Media, J. Chem. Eng. Jpn. 26, 3 (1993) 297-302. doi: 10.1252/jcej.26.29.

[24] A. Acharya, R. Mashelkar, J. Ulbrecht, Mechanics of bubble motion and deformation in non-newtonian media, Chem. Eng. Sci. 32, 8 (1977) 863-872. doi: 10.1016/0009-2509(77)80072-9.

[25] A. Drews, H. Prieske, M. Kraume, Optimierung der Blasen- und Zirkulationsströmung in Membranbelebungsreaktoren (in German), Chem. Ing. Tech. 80, 12 (2008) 1795–1801. doi: 10.1002/cite.200800149.

[26] B. Figueroa-Espinoza, R. Zenit, D. Legendre, The effect of confinement on the motion of a single clean bubble, J. Fluid Mech. 616, (2008) 419-443. doi: 10.1017/S0022112008004072.

[27] A. Tokuhiro, M. Maekawa, K. Iizuka, K. Hishida, M. Maeda, Turbulent flow past a bubble and an ellipsoid using shadow-image and PIV techniques, Int. J. Multiphase Flow 24, 8 (1998) 1383-1406. doi: 10.1016/S0301-9322(98)00024-X.

[28] A. Fujiwara, A. Tokuhiro, K. Hishida, Application of PIV/LIF and Shadow-Image to a Bubble Rising in a Linear Shear Flow Field, 10th Int Symp on Applications of Laser Techniques to Fluid Mechanics, 2000.

[29] A. Fujiwara, Y. Danmoto, K. Hishida, Bubble Deformation and Surrounding Flow Structure Measured by PIV/LIF and Shadow Image Technique, ASME Conference Proceedings, 2003.

[30] D. Funfschilling, H. Li, Flow of non-Newtonian fluids around bubbles: PIV measurements and birefringence visualisation, Chem. Eng. Sci. 56, 3 (2001) 1137-1141. doi: 10.1016/S0009-2509(00)00332-8.

[31] X. Frank, H. Z. Li, D. Funfschilling, F. Burdin, Y. Ma, Bubble Motion in Non-Newtonian Fluids and Suspensions, Can. J. Chem. Eng. 81, 3-4 (2003) 483-490. doi: 10.1002/cjce.5450810321.

[32] D. Funfschilling, H. Li, Effects of the Injection Period on the Rise Velocity and Shape of a Bubble in a Non-Newtonian Fluid, Chem. Eng. Res. Des. 84, 10 (2006) 875-883. doi: 10.1205/cherd.01229.

[33] H. Z. Li, X. Frank, D. Funfschilling, P. Diard, Bubbles' rising dynamics in polymeric solutions, Phys. Lett. A 325, 1 (2004) 43-50. doi: 10.1016/j.physleta.2004.03.023.

[34] C. Brücker, Structure and dynamics of the wake of bubbles and its relevance for bubble interaction, Phys. Fluids 11, 7 (1999) 1781-1796. doi: 10.1063/1.870043.

[35] Y.-A. Hassan, J. Ortiz-Villafuerte, W.-D. Schmidl, Three-dimensional measurements of single bubble dynamics in a small diameter pipe using stereoscopic Particle Iimage Velocimetry, Int. J. Multiphase Flow 27, 5 (2001) 817-842. doi: 10.1016/S0301-9322(00)00054-9.

[36] J. Ortiz-Villafuerte, W. D. Schmidl, Y. A. Hassan, Three-dimensional PTV study of the surrounding flow and wake of a bubble rising in a stagnant liquid, Exp. Fluids 29, 1 (2000) 202-210. doi: 10.1007/s003480070022.

[37] K. Dewsbury, D. Karamanev and A. Margaritis, Hydrodynamic characteristics of free rise of light solid particles and gas bubbles in non-Newtonian liquids, Chem. Eng. Sci. 54, 21 (1999) 4825-4830. doi: 10.1016/S0009-2509(99)00200-6.

[38] N. M. S. Hassan, M. M. K. Khan, M. G. Rasul, D. W. Rackemann, An Experimental Investigation of Bubble Rise Characteristics in a Crystal Suspended Non-Newtonian Fluid, AIP Conference Proceedings 1027, 1 (2008) 743-745. doi: 10.1063/1.2964831.

[39] Z. Liu, Y. Zheng, L. Jia, Q. Zhang, Study of bubble induced flow structure using PIV, Chem. Eng. Sci. 60, 13 (2005) 3537-3552. doi: 10.1016/j.ces.2004.03.049.

[40] C. Maneri, N. Zuber, An experimental study of plane bubbles rising at inclination, Int. J. Multiphase Flow 1, 5 (1974) 623-645. doi: DOI: 10.1016/0301-9322(74)90022-6.

[41] K. Sakakibara, M. Yamada, Y. Miyamoto, T. Saito, Measurement of the surrounding liquid motion of a single rising bubble using a Dual-Camera PIV system, Flow Meas. Instrum. 18, 5-6 (2007) 211-215. doi: 10.1016/j.flowmeasinst.2007.07.003.

[42] T. Saito, K. Sakakibara, Y. Miyamoto, M. Yamada, A study of surfactant effects on the liquid-phase motion around a zigzagging-ascent bubble using a recursive cross-correlation PIV, Chem. Eng. J. 158, 1 (2010) 39-50. doi: 10.1016/j.cej.2008.07.021.

[43] K. Yoshimoto, T. Saito, 3-dimensional liquid motion around a zigzagging ascent bubble measured using tomographic Stereo PIV, Proceedings of the 15th International Symposium on Applications of laser techniques to Fluid mechanics, 2010.

[44] M. J. Sathe, C. S. Mathpati, S. S. Deshpande, Z. Khan, K. Ekambara, J. B. Joshi, Investigation of flow structures and transport phenomena in bubble columns using Particle Image Velocimetry and miniature pressure sensors, Chem. Eng. Sci. 66, 14 (2011) 3087-3107. doi: 10.1016/j.ces.2011.04.002.

[45] S. Takagi, Y. Matsumoto, Surfactant effects on bubble motion and bubbly flows, Annu. Rev. Fluid Mech. 43, (2011) 615-636. doi: 10.1146/annurev-fluid-122109-160756.

[46] A. W. G. de Vries, A. Biesheuvel, L. Wijngaardenvan, Notes on the path and wake of a gas bubble rising in pure water, Int. J. Multiphase Flow 28, 11 (2002) 1823-1835. doi: DOI: 10.1016/S0301-9322(02)00036-8.

[47] L. Zhang, C. Yang, Z.-S. Mao, Unsteady motion of a single bubble in highly viscous liquid and empirical correlation of drag coefficient, Chem. Eng. Sci. 63, 8 (2008) 2099-2106. doi: DOI: 10.1016/j.ces.2008.01.010.

[48] H. Brauer, Particle/Fluid transport processes, in: Fortschritte der Verfahrenstechnik Vol. 17, VDI-Verlag, 1979.

Figure 1

Click here to download high resolution image

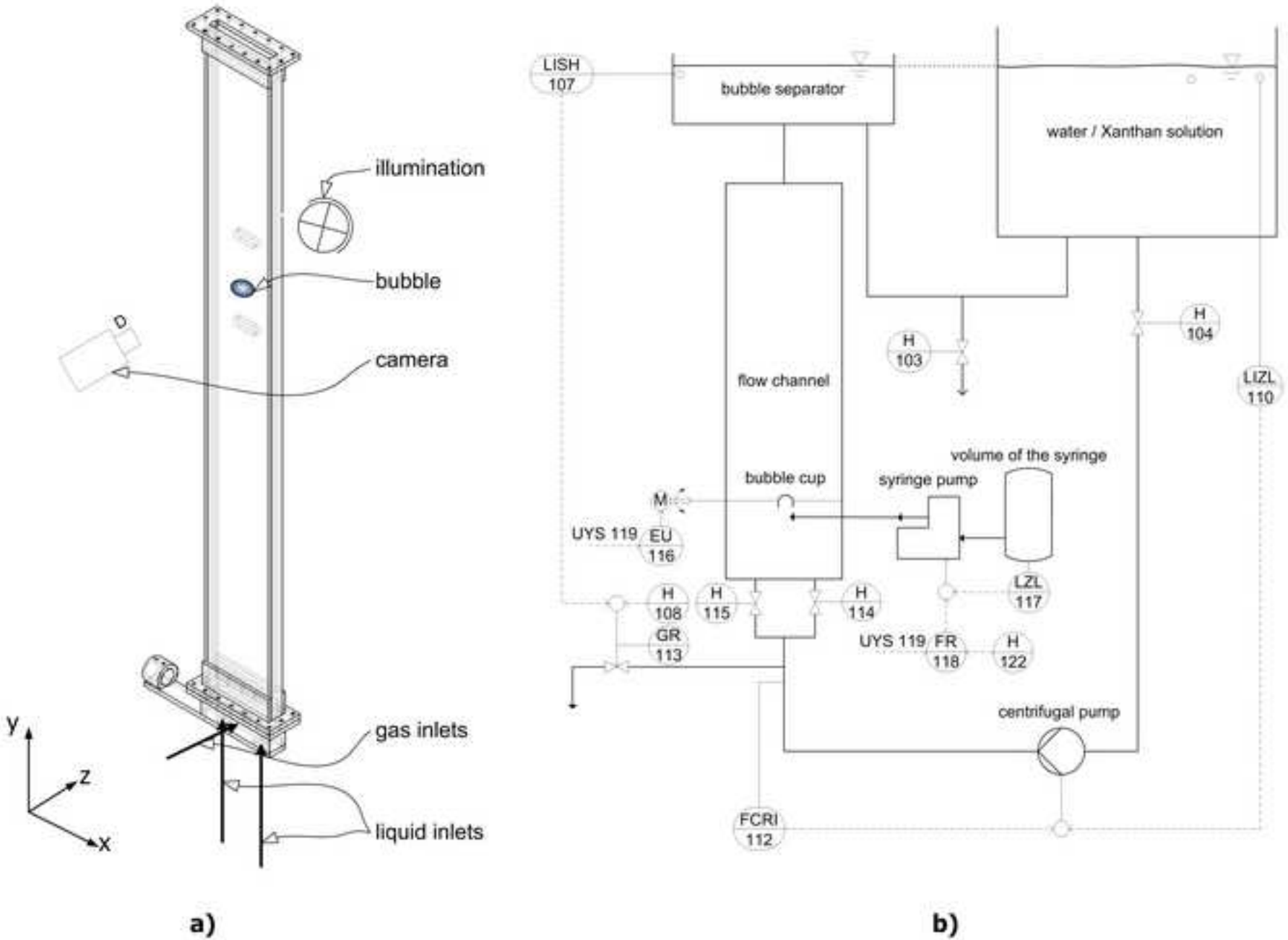

Figure 2

Click here to download high resolution image

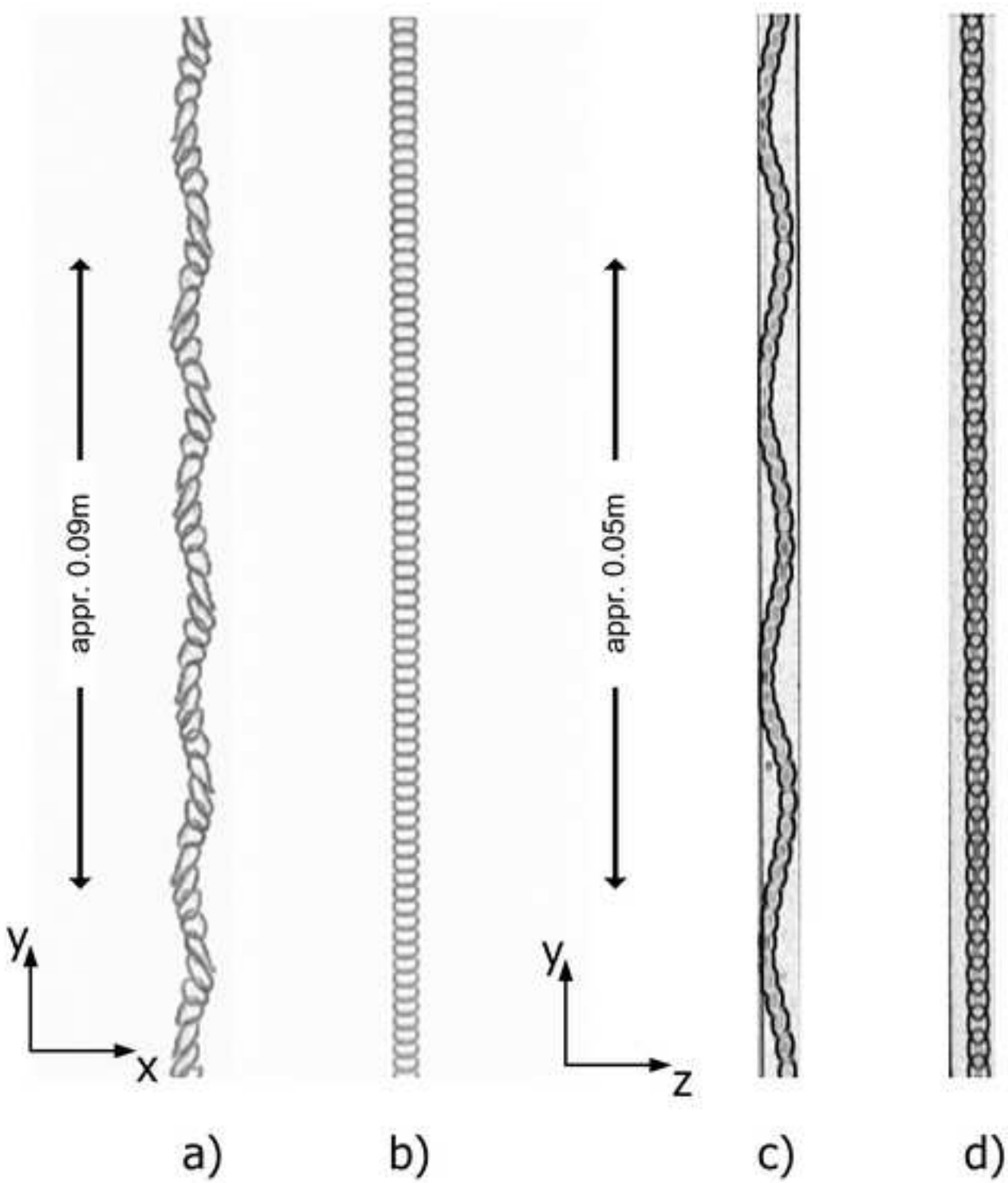

Figure 3

Click here to download high resolution image

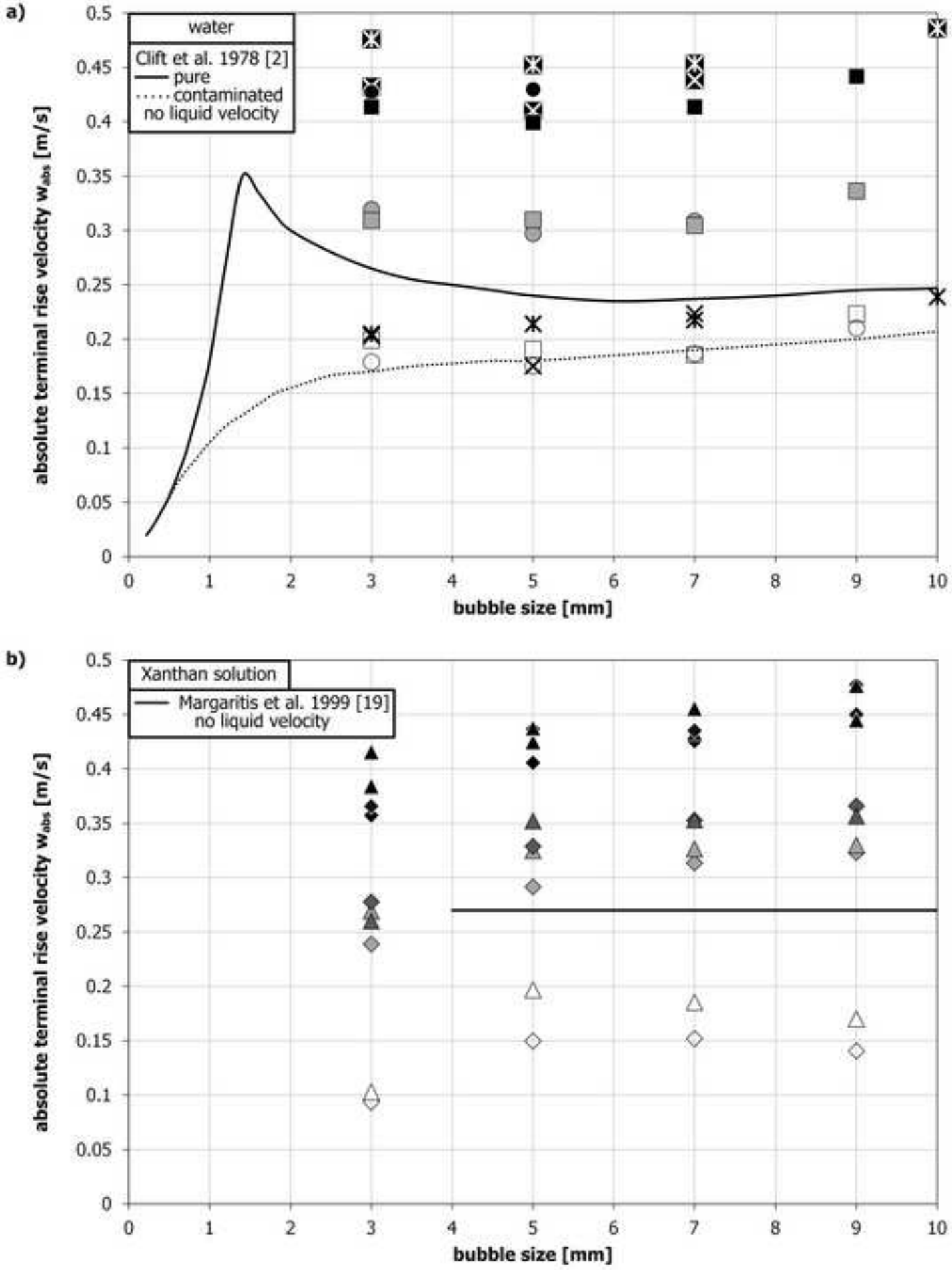

Figure 4

Click here to download high resolution image

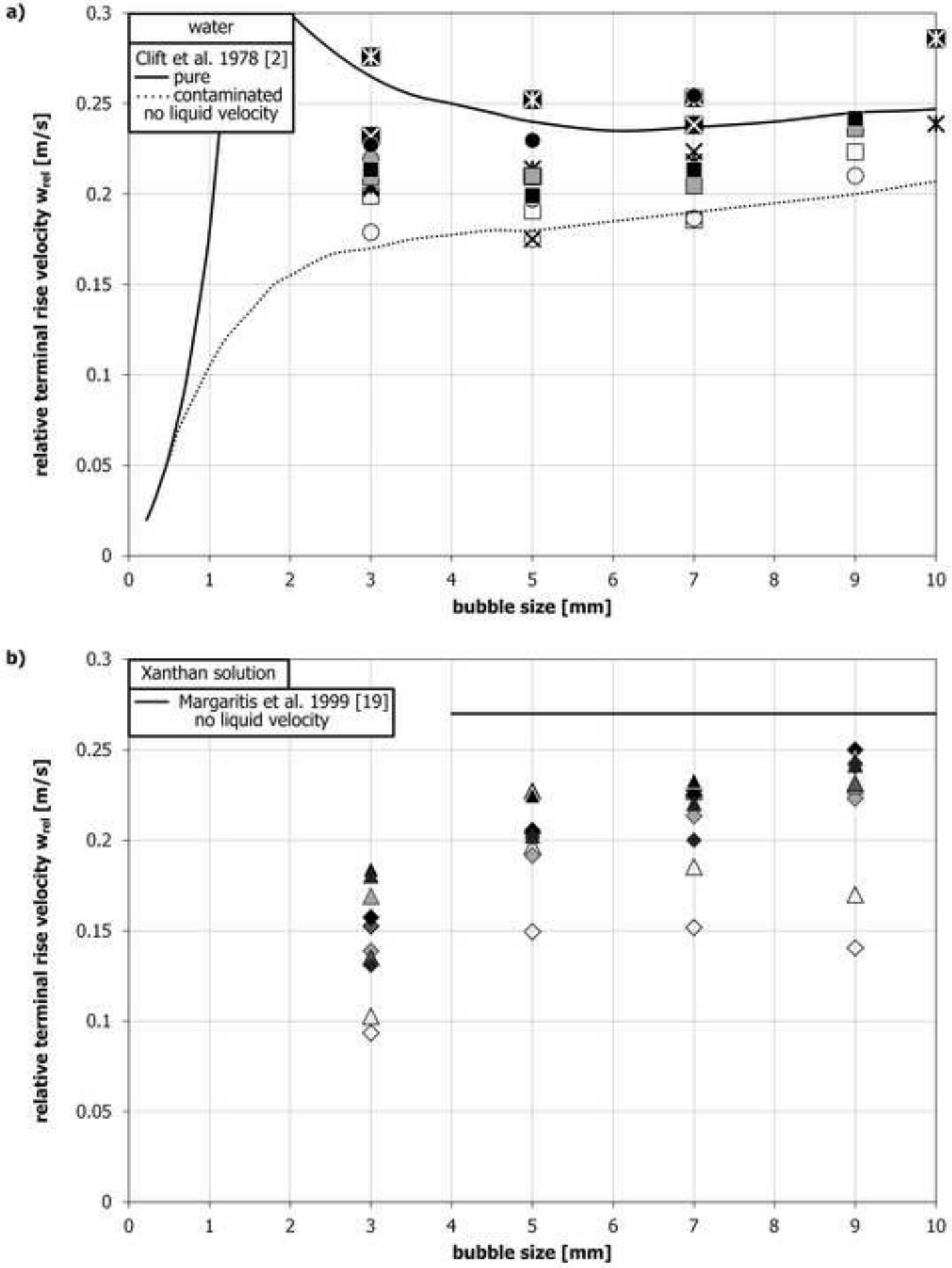

Figure 5

Click here to download high resolution image

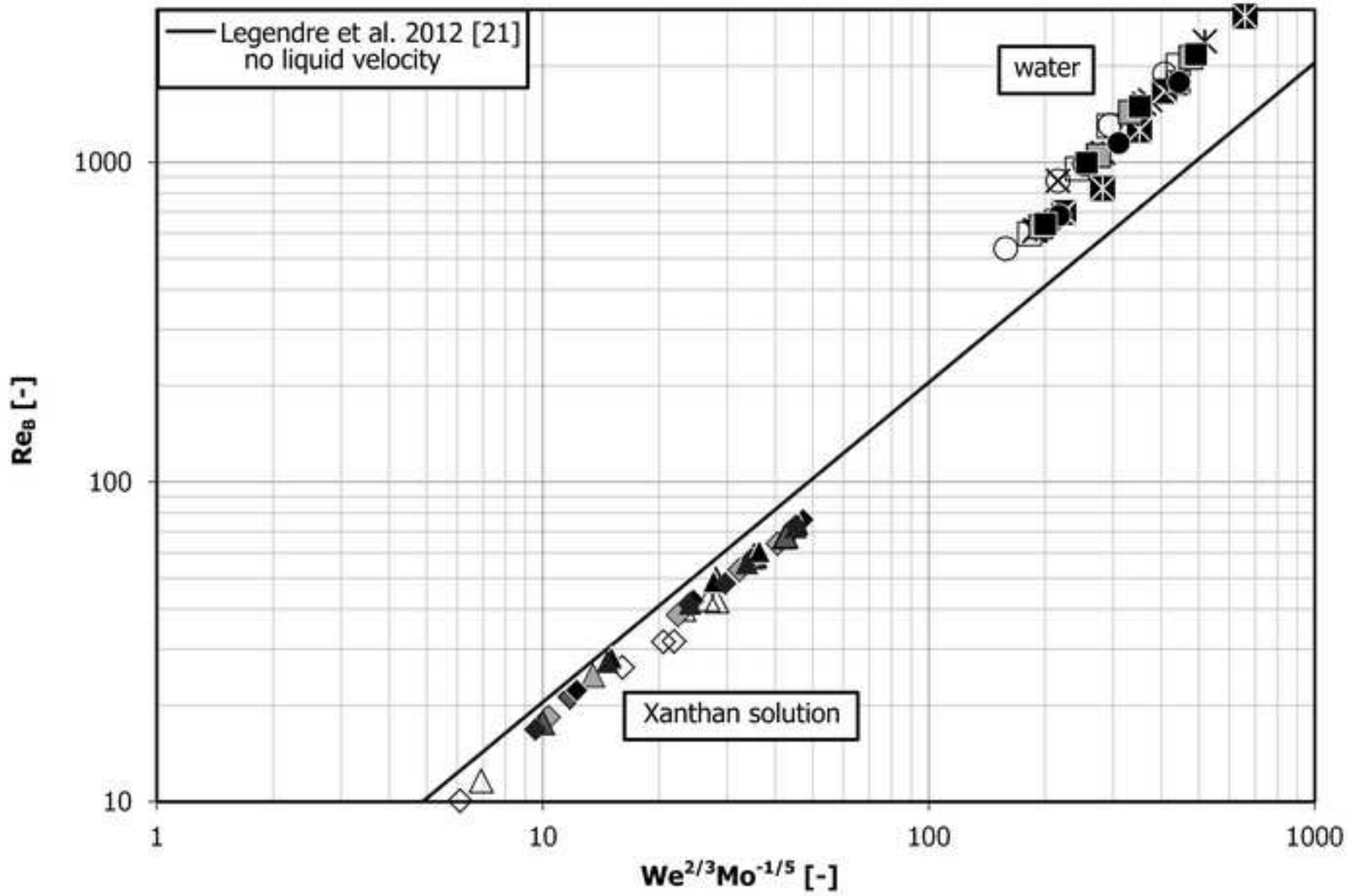

Figure 6

Click here to download high resolution image

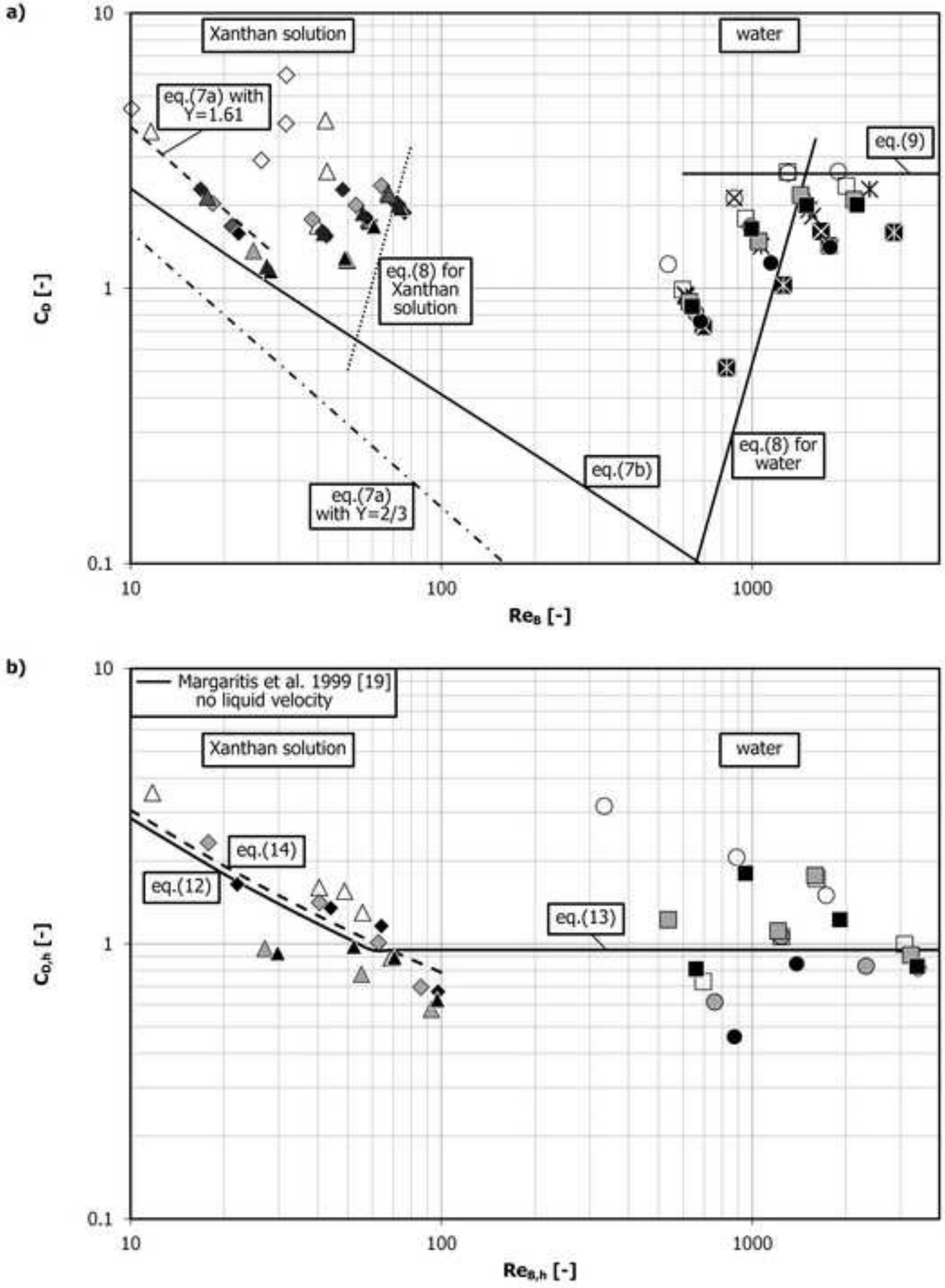

Figure 7

Click here to download high resolution image

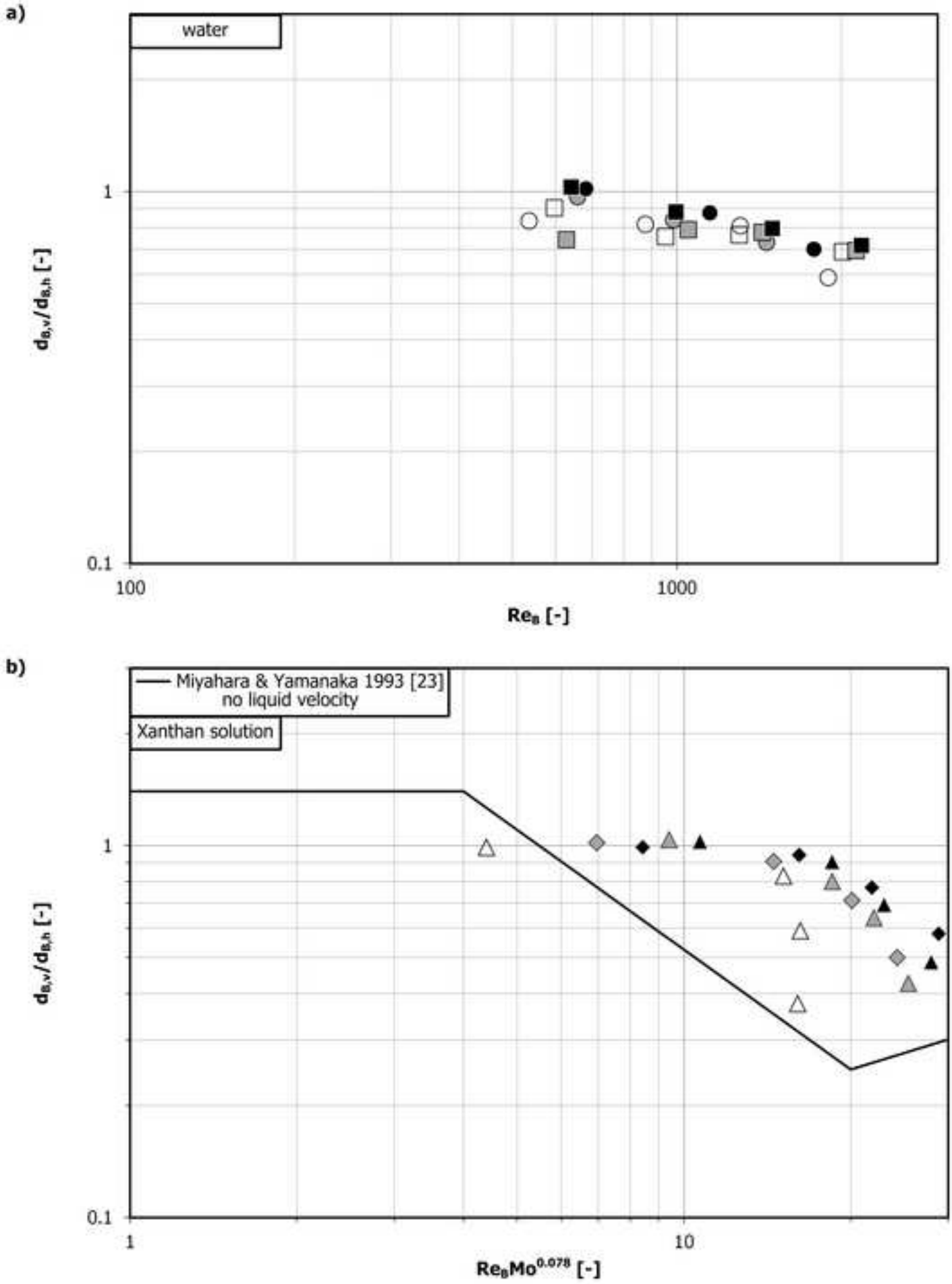

Figure 8

Click here to download high resolution image

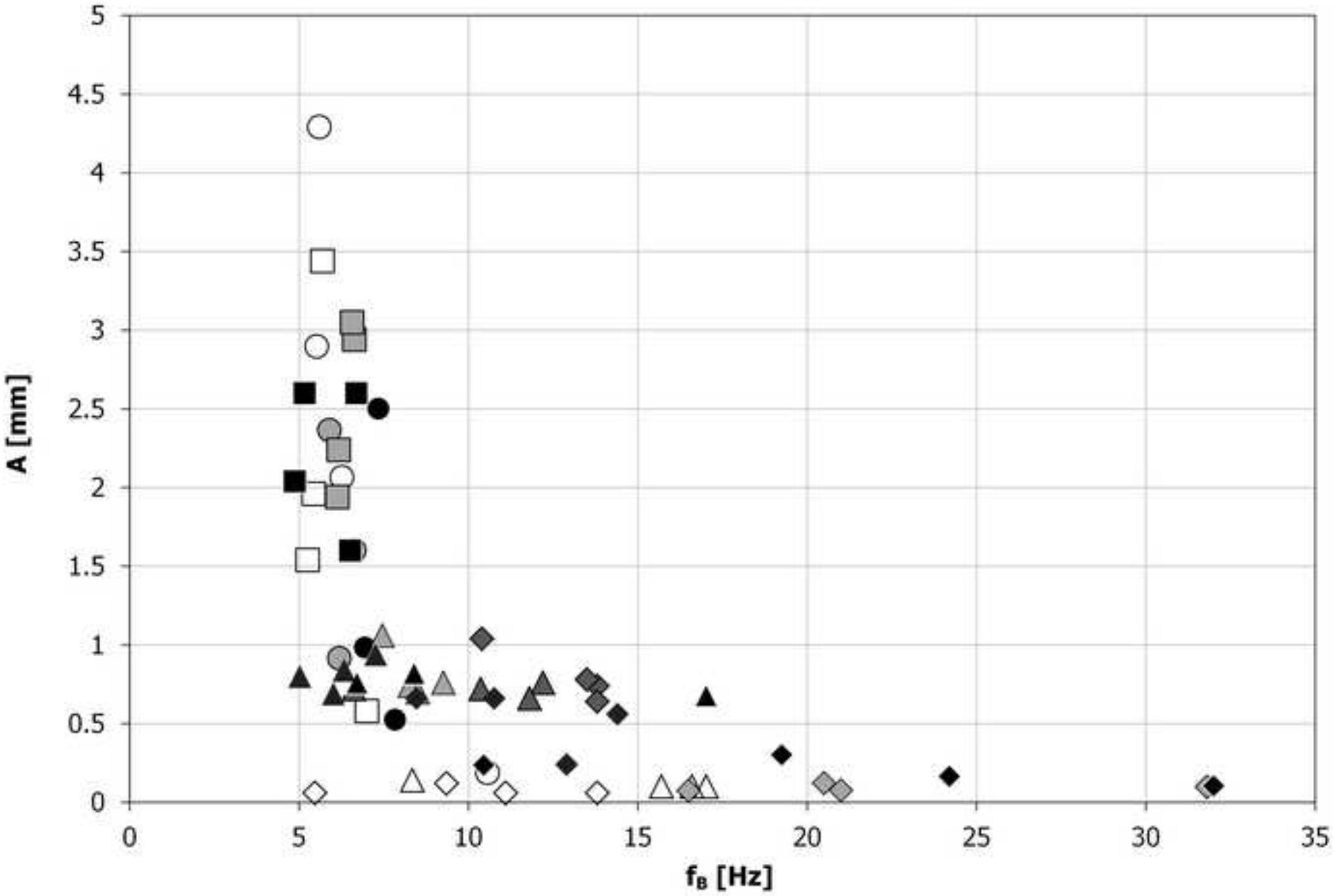

Figure 9

Click here to download high resolution image

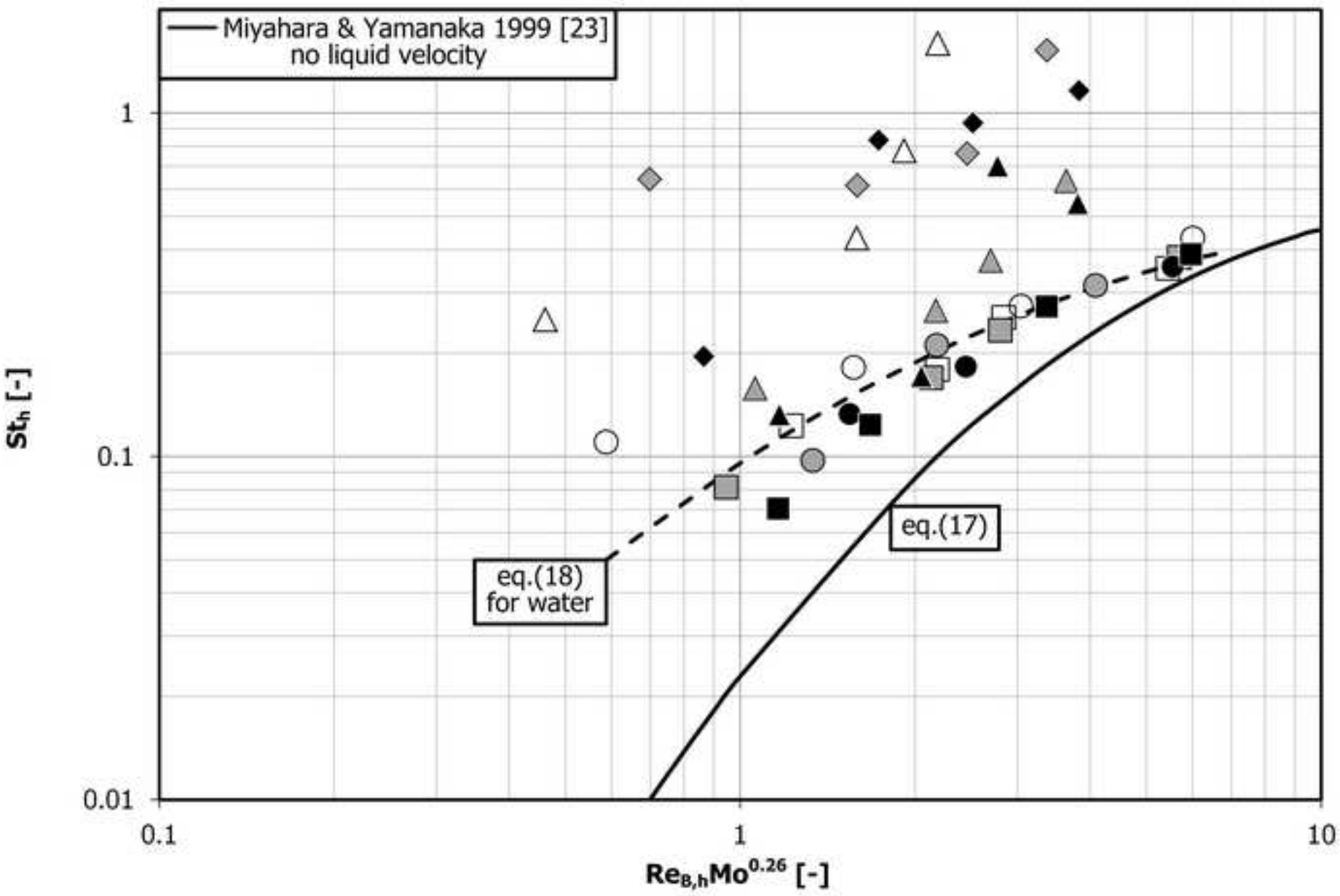

Figure 10
Click here to download high resolution image

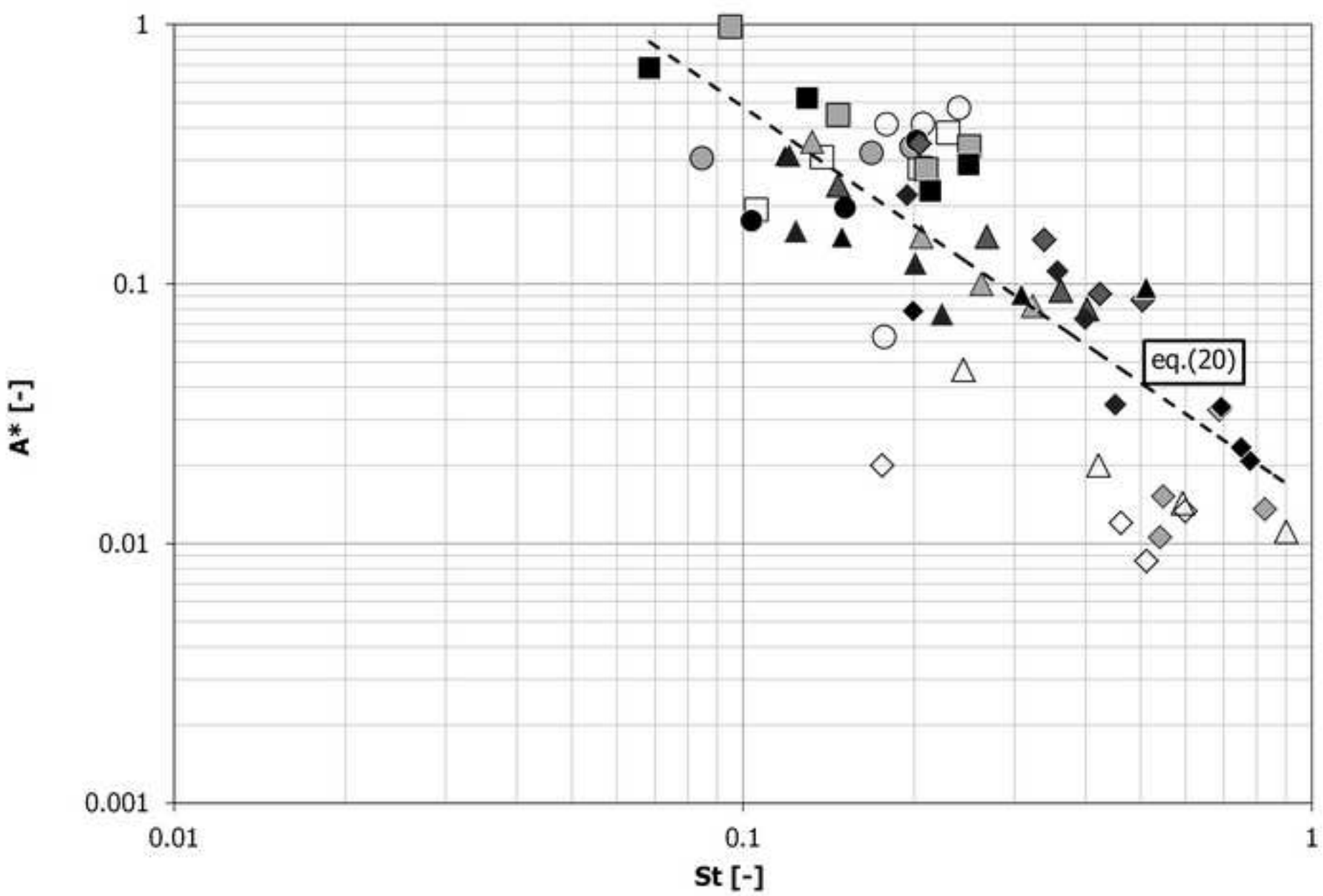

Table 1

Table 1: Publications dealing with the rise of single bubbles in liquid and important related publications

Reference	High speed camera setup	Setup geometry (cyl.: i.d. x h, rect.: w x d x h)	Bubble size	Varied parameters	Measured quantity	Comment / Brief results
[24]	- / -	rectangular 165x165x245 mm³	-	injector type	bubble velocity, shape, deformation	- / -
[13]	- / 25 Hz	several	Taylor bubbles	geometry, viscosity	bubble velocity	Taylor bubbles / -
[6]	- / 6 Hz	rectangular 230x230x772 mm³	2.6-26.7 mm	bubble size, viscosity	bubble velocity	investigation of coalescence / -
[20, 25]	752x582 pixel² / 350 Hz	rectangular 3-11x160x700 mm³	3-24 mm	bubble size, viscosity	bubble velocity	- / -
[7]	- / 1 kHz	rectangular 150x150x650 mm³	2.48 mm	-	rising path, shape	- / -
[26]	- / -	rectangular 3.6-4.7x200x400 mm³	<1.4 mm	Re	rising path	- / drag coefficients
[27]	768x493 pixel² / shadowgraphy	rectangular 100x100x1000 mm³	9.12 mm	investigation of a bubble and a solid particle	shape, rising path	counter current flow cell / -
[28]			8 mm	viscosity		one side of the channel is a movable belt / influence of the shear flow field on the rising path
[9, 29]	+ 2nd shadowgraphy camera for 3D bubble shape reconstruction		2-6 mm	bubble size		+ 3D bubble shape

Reference	High speed camera setup	Setup geometry	Bubble size	Varied parameters	Measured quantity	Comment / Brief results
[30]	- / -	rectangular 60x60x500 mm³	<12 mm	viscosity	shape, bubble velocity, coalescence behavior	- / bubble interaction
[31, 32]		cylindrical 300x500 mm²	3-14 mm			
[33]		cylindrical 300x1500 mm²	6.5-7.2 mm			
[34]	512x512 pixel² / shadowgraphy	rectangular 100x100x1200 mm³	5-7 mm	bubble size	rising path, oscillation frequency, shape, bubble velocity	counter current flow cell / physical description of the bubble behavior during its ascent
[35, 36]	640x480 pixel² / shadowgraphy, 2D hybrid particle tracking and 3D reconstruction	cylindrical 12.7x1300 mm²	3 mm	-	rising path, bubble velocity	stagnant water / physical description of the bubble behavior during its ascent
[37, 38]	- / -	rectangular 300x300x240mm³	1.5-33 mm	Re number	bubble velocity	- / -
[39]	1200x1600 pixel² / shadowgraphy	rectangular 68x88x450mm³	~6 mm	viscosity, gas flow rate	rising path, shape	bubble train / influence of the viscosity on the rising path
[40]	- / -	rectangular 9.5-1.3x63-86x914mm³	<55 mm	channel inclination, viscosity	bubble velocity	/ viscosity influences bubble velocity for inclined channels

Reference	High speed camera setup	Setup geometry	Bubble size	Varied parameters	Measured quantity	Comment / Brief results
[23]	- / -	cylindrical 10x1000mm²	2-30 mm	viscosity	shape, bubble velocity, oscillation	- / -
[4]	1280x1024 pixel² / 500 Hz	Rectangular 1x400x800mm³	2.6-8.3 mm	bubble size, channel inclination	shape, bubble velocity, oscillation	- / -
[8]	2 times 512x512 pixel² / 1 kHz	rectangular 150x150x400mm³	0.66-0.93 mm	bubble size, viscosity	shape, rising path	- / -
[41]	960x960 pixel² / shadowgraphy	rectangular 150x150x270/500mm³	~2.9 mm	-	rising path, shape	- / -
[42]				surfactant concentration		- / influence of surfactants on bubble motion
[43]	1024x1024 pixel² / shadowgraphy	octagon, 160x160x230mm³		-		- / relation between bubble shape, velocity and path
[11]	2048x2048 pixel² / shadowgraphy	rectangular 200x15x500 mm³	0.1-15 mm	bubble size, liquid velocity	shape	bubbly flow / comparison between single bubble behavior and bubble swarms
[44]		+ cylindrical 150x650mm²	-	geometry		bubbly flow / -
[5]		rectangular 200x15x1000 mm³	2-35 mm	bubble size	bubble diameter	bubbly flow / -
[45]	-	-	-	-	-	Review / influence of surfactants
[46]	-	rectangular 15x15x500mm³	0.8-1.8 mm	bubble size	rising path	- / Wall interaction

Reference	High speed camera setup	Setup geometry	Bubble size	Varied parameters	Measured quantity	Comment / Brief results
[12]	- / 955 Hz	rectangular 15x300x2000mm	15-80 mm	bubble size	shape, bubble velocity	Comparison with CFD / -
[10]	2times 1280x1024 pixel² / 500 Hz	rectangular 50x50x1300mm³	1-4 mm	bubble size	rising path	With superimposed liquid velocity / -
[47]	752x582 pixel² / -	rectangular 210x210x600mm³	2.7-5.2 mm	bubble size, viscosity	bubble velocity, bubble size	- / -

d: diameter; h: height; i.d.: inner diameter; w: width

Table 2

Table 2: Tested parameter combinations (S: CFD in water, W: water, X: Xanthan solution, -: not tested)

channel depth [mm]		5										7									
v_L [cm/s]		0			10		12.5		20			23.5		0			10		12.5		20			23.5	
continuous phase / simulation		W	X	S	W	X	W	X	W	X	S	W	X	W	X	S	W	X	W	X	W	X	S	W	X
bubble size [mm]	3	○	◇	×	○	◇	-	◈	●	◆	⊠	-	◈	□	△	✳	▨	△	-	▲	■	▲	⊠	-	▲
	5	○	◇	×	○	◇	-	◈	●	◆	⊠	-	◈	□	△	✳	▨	△	-	▲	■	▲	⊠	-	▲
	7	○	◇	×	○	◇	-	◈	●	◆	⊠	-	◈	□	△	✳	▨	△	-	▲	■	▲	⊠	-	▲
	9	○	◇	-	-	◇	-	◈	-	◆	-	-	◈	□	△	-	▨	△	-	▲	■	▲	-	-	▲
	10	-	-	-	-	-	-	-	-	-	-	-	-	-	-	✳	-	-	-	-	-	-	⊠	-	-